A strain rate dependent model with decreasing Young's Modulus for cortical human bone

D. Sánchez-Molina[a]*, S. García-Vilana[a],
L. Martínez-Sáez[b], J. Llumà[a]

May 11, 2023

[a]UPC, GRABI, Eduard Maristany, 16, 08036 Barcelona
[b]UPM-INSIA, Crtra. Valencia, km.7, 28031 Madrid

Abstract

In the existing literature, some studies have observed an increase in the elastic modulus of human cortical bone with strain rate, which has been described as a consequence of the viscoelastic properties of the bone. However, these results contradict the findings of other studies, in which an independence or decrease of the elastic modulus with strain rate is observed, which could be explained by other non-viscoelastic mechanisms. This research studies the dynamic behavior of human cortical bone specimens and investigates their mechanical properties. A full and objective strain rate dependent model is proposed and used to describe the experimental results obtained from uniaxial tensile tests of twenty-one human rib cortical bone specimens from twelve male post mortem human subjects (average age of 68.5 ± 12.3 years). In addition, a general discussion of some families of viscoelastic models is given and the caution with which they should be used when dealing with complex materials such as bone. The main experimental finding is that in the range of strain rate analyzed ($\dot{\varepsilon}$ = 0.10 – 0.60), there is a significant decrease in Young's modulus ($E \approx 18$ GPa for $\dot{\varepsilon} = 0.10$ s^{-1} and $E \approx 8$ GPa for $\dot{\varepsilon} = 0.50$ s^{-1}), which is not of viscoelastic origin. Moreover, the most frequently used

*Corresponding author: david.sanchez-molina@upc.edu

viscoelastic models analyzed in this study predict how the elastic modulus should not vary markedly with strain rate for small strains. In fact, the observed behavior seems related to the findings of other researchers who observed that the microcraking damage depends on the strain rate in the same sense found in our work. This allows us to interpret the qualitative results as a consequence of the microcracking that takes place within the cortical bone, and not related to viscoelastic effects.

KEYWORDS: Strain rate dependent materials, Bone, Constitutive model, Tissue Characerization, Viscoelasticity.

Nomenclature

DIC - Digital Image Correlation
QLVE - Quasi-Linear Viscoelastic
ROI - Region of Interest
SEDF - Strain Energy Density Function
YM - Young's modulus

1 Introduction

Like many other materials, human cortical bone exhibits some variation in its mechanical properties when measured over a wide range of strain rate. In particular, many researchers have found evidence of apparent viscoelastic behavior in bone [1, 2, 3, 4, 5, 6, 7, 8] and, consequently, some viscoelastoplastic models [9, 10, 11] have been proposed for compact bone. Although the viscoelastic/viscoplastic models are a particular case of strain rate dependent constitutive models, these types of models do not exhaust all the possible strain rate dependent behaviors.

Several authors assumed that in a viscoelastic model the YM should increase with strain rate following pioneering works such as those of McElhaney [1] or Wood [2]. However, many contemporary researchers did not find any evidence that the tangent YM increases significantly with strain rate in some tissues, even when other mechanical properties did change [4, 6, 12, 13, 14, 15, 16, 17]. Other researchers only have found that YM increases very slightly [18] and some authors even noticed in their experi-

mental data that in certain specific strain rate ranges YM seems to decrease [5, 8, 19, 20], as shown in figure 1. This is consistent with a detailed calculation which shows that in a wide class of viscoelastic models, extensively used in the literature, YM should be constant or highly insensitive to strain rate.

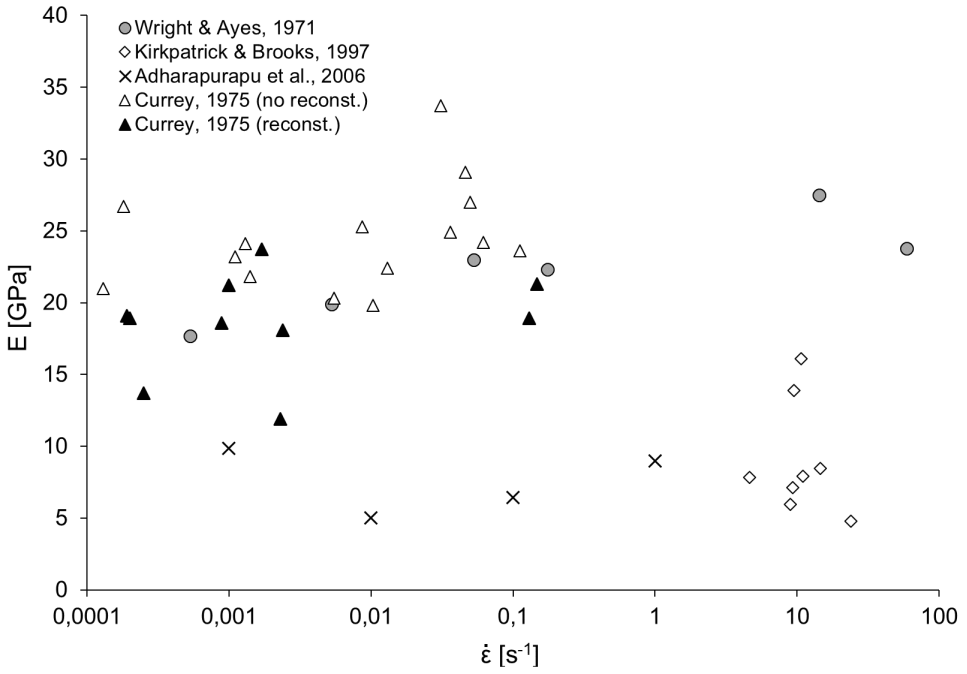

Figure 1: Comparison of literature studies reporting YM of cortical bone at different strain rates within the range of the present study. This comparison shows that there is no consistently monotonic increase in YM with strain rate, which has been corroborated computing the p-values [Wright & Ayes, 1971($p = 0.436$), Kirkpatrick & Brooks, 1997 ($p = 0.447$), Adharapurapu et al., 2006 ($p = 0.613$), Currey, 1975 no Haversian reconstruction ($p = 0.337$), Haversian reconstruction ($p = 0.494$), all specimens ($p = 0.448$)].

In light of the disparate trends observed between YM and strain rate in previous studies. this research focuses on the dependence of YM on strain rate in human cortical bone. Specifically, this study aims to demonstrate that viscoelasticity is not the primary mechanism underlying the observed increase in YM with strain rate, but rather another strain-rate dependent phenomenon, which could explain the observed decrease in YM in some studies. To do this, the present research is divided in an experimental part and a theoretical analysis part. In our experimental work, we found that over a

reduced strain rate range, YM decreased significantly, and it is supposed to be related to microcracking damage. We conjectured that this experimental finding was due to the fact that microcraking is strain rate dependent, as some researchers established [22]. So, this microcracking effect could explain why some decreasing trends of YM with strain rate are observed in some ranges. This effect is obviously not of viscoelastic origin, although it requires a strain rate dependent model. For this reason, a phenomenological full constitutive model of this type is proposed in this paper, which adequately fits the data of experiments with cortical bone samples from human ribs. The model satisfies the objectivity requirements and can be easily generalized to three-dimensional load cases, although we have applied it lately to uniaxial tensile tests.

In addition, an analysis of the behavior of widely known models, summarized in [21], is provided to justify rigorously that no significant increase in the YM can be expected for low strain regime with these models. This suggests that, in certain cases, the modest apparent increase in YM may well be an experimental artifact due to the use of an inappropriate strain range to estimate YM, thus taking into account a widest curve area to compute YM. Estimating YM with data near the origin of coordinates allowed us to obtain a well defined tangent YM, while when data far from the same origin are considered, a secant YM is obtained. The tangent YM does not vary with strain rate, although its approximation, the secant YM, would show a modest increase. The approximation of intrinsic/tangent YM for the apparent/secant YM could account for the apparent increase in modulus observed in some pioneering work based on analog data rather than digital data. All those aspects are treated along the present research.

2 Data and Methods

2.1 Material and specimen preparation

The material used in this study consisted of a sample of human rib specimens harvested from forensic autopsies conducted at the Forensic Pathology Service of the Legal Medicine and Forensic Science Institute of Catalonia (FPS/IMLCFC). All the specimens were initially removed for complementary medical-legal investigation. This study was approved by the Research and Ethics Committee of the IMLCFC. Subjects whose cause of death was

trauma or precipitation, as well as those with known bone pathology, were excluded.

Thirteen healthy 4th ribs were obtained from autopsies of twelve male caucasian *post mortem* human subjects (PMHS) with an average age of 68.5±12.3 years and a BMI of 26.0±5.8 kg/m^2. From these ribs twenty-one coupons were machined following the same methodology described in previous work of the authors of this study [23, 24, 25]. The specimens were classified according to the anatomical region of the rib in anterior (A), lateral (B) or posterior (C). Each coupon specimen was subjected to an uniaxial tensile test to complete fracture.

Once received, the ribs were wrapped in saline soaked gauze and stored in airlock plastic bags in a freezer at a temperature of –20°C. Then, bone coupons were machined from entire ribs (Figure 2(a)), following the method described in previous studies [23, 24].

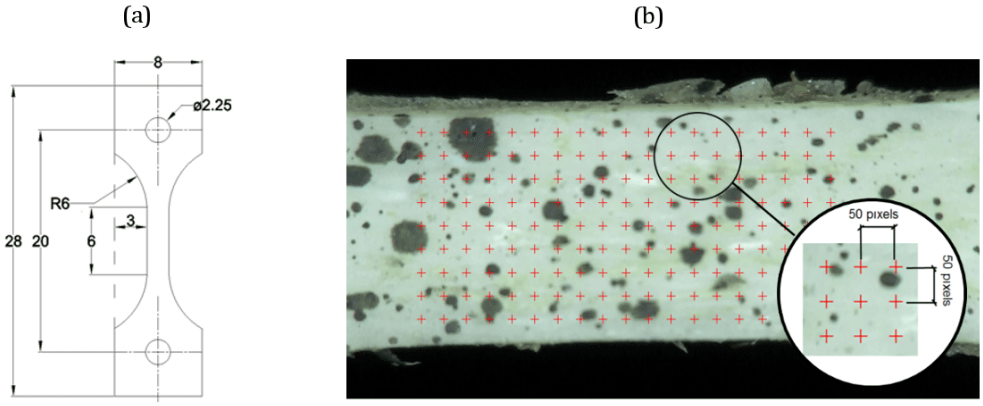

Figure 2: (a) Coupon dimensions for the specimens machined from rib cortical bone. (b) The initial grid used for defining a collection of material points which will be tracked during the elongation of the sample. Points are separated between them 50 pixels.

2.2 Tensile tests, data processing and Digital Image Correlation

The tensile tests were performed with a ZwickRoell ProLine® and applied load was measured using a load cell HBM S9M® of 500 N coupled to a data acquisition system Spider 8-30 from HBM®. The strain rate of the different tests ranged from $\dot{\varepsilon} = 0.08$ to 0.60 s^{-1} (within this range, a constant $\dot{\varepsilon}$

could be ensured throughout the test, and tests were performed at different strain rates to analyze its influence on YM, see Table 1). Special fixtures were used which had longitudinal slotted holes to allow the machine to reach the intended speed before exerting the load, and displacement was carefully measured to ensure that the strain rate was constant. The strain was computed from a high-speed video recording of the ROI (gauge length of the coupons) during the whole test, see figure 2(b). The recording was made with a high-speed camera PCO 1200s (around 1000 fps), according to the procedure of [24, 25]. This video was analyzed using a Digital Image Correlation (DIC) motion tracking software from MATLAB® to obtain the strain in each moment of the test. To do this, a mesh of points was generated on the ROI in the gauge length.

The DIC procedure provided the position of the mesh points (Figure 2) in each frame and, thus, the elongations of the specimen could be determined and the Finite Strain Theory can be applied [27], see equation (1). In particular, the components of the *material* or *Green-Lagrange strain* tensor can be computed by means of the following equation:

$$E_{ij} = \frac{1}{2}\left(\frac{\partial u_i}{\partial x_j} + \frac{\partial u_i}{\partial x_j} + \sum_k \frac{\partial u_k}{\partial x_i}\frac{\partial u_k}{\partial x_j}\right) \tag{1}$$

for $i, j \in \{1, 2\}$ [being $x_1 = x$ and $x_2 = y$]. In practice, the values of the derivatives $\partial u_i/\partial x_j$ are obtained by means of regression analysis at each step, computing the slope of the curves of displacement $u_i(x, y, z)$. This procedure provides both longitudinal and transversal strain values during the whole test, which were related to the stress values applied. Specifically, stresses were computed as the force divided by the initial area, since the low deformation of bone, usually under 4%, does not significantly affect the cross-section. Moreover, from the stress-strain curves, the maximum stress and maximum strain were determined, as well as Young Modulus (YM) which was computed as the slope of the initial linear region of the stress-strain curve.

2.3 The proposed strain rate dependent model

To explain the experimental data of this study, a strain rate dependent model is proposed that aims to describe the experimental results (see next section). This model cannot be considered as viscoelastic, because it does not represent an increase of stress with strain rate as the usual viscoelastic models

do. Instead of this, the model uses the assumption that the axial stress is a sum of a *purely elastic contribution* of the type $\sigma = \sigma_0(\varepsilon) + \sigma_d(\varepsilon, \dot{\varepsilon})$, only depending on the longitudinal strain ε, and a *strain rate dependent contribution* also depending on the strain rate $\dot{\varepsilon}$, see equation (2). Here we present the particularization of the full 3D model to the uniaxial tensile test; the full 3D model is summarized in appendix 8.

Following the standard procedure of Coleman and Noll [26, 27], it can be found a Strain Energy Density Function (SEDF) that also admits the decomposition $w(\varepsilon, \dot{\varepsilon}) = w_0(\varepsilon) + w_d(\varepsilon, \dot{\varepsilon})$, and thus the stress σ can be found as:

$$\sigma = \frac{\partial w}{\partial \varepsilon} = \frac{\partial w_0(\varepsilon)}{\partial \varepsilon} + \frac{\partial w_d(\varepsilon, \dot{\varepsilon})}{\partial \varepsilon} = \sigma_0(\varepsilon) + \sigma_d(\varepsilon, \dot{\varepsilon}) \tag{2}$$

A convenient mathematical form for $w(\varepsilon, \dot{\varepsilon})$ is obtained from the *objectivity principle*, which requires that this SEDF is a function of the algebraic invariants of the strain tensor $\mathbf{E}$ which are compatible with the symmetry of the material [27, 28]. Essentially, the objectivity principle and material symmetry considerations lead to a SEDF which can be expressed as a function of certain algebraic invariants, as equation (3), which guarantees that the constitutive laws retain the same general form for different reference frames. More specifically, the above considerations lead to a mathematical form $w = w_0(\{I_p\}) + w_d(\{I_p, J_q\})$ where $I_p(\varepsilon)$ are invariants of the deformation tensor and $J_q(\varepsilon, \dot{\varepsilon})$ are invariants formed from the deformation tensor and its time derivative (see section 8). Since the human rib can be adequately modeled as a transversely isotropic material, its symmetry group is SO(2) and the descriptions in [28] led to the following elastic invariants:

$$\begin{aligned} I_1 &= 3 + 2\left(1 + 2\nu_T\right)\varepsilon, & I_4 &= 1 + 2\varepsilon, \\ I_2 &= 3 + \left(4 - 8\nu_T\right)\varepsilon + \left(4\nu_T - 8\right)\nu_T\varepsilon^2, & I_5 &= \left(1 + 2\varepsilon\right)^2, \\ I_3 &= \left(1 + 2\varepsilon\right)\left(1 + 2\nu_T\varepsilon\right)^2 \end{aligned} \tag{3}$$

These invariants are the reduced forms of the invariants in equations (16), explained in the appendix (section 8), I_1, I_2, I_3 are compatible with any rotation, while I_4, I_5 are compatible with any rotation around the material symmetry axis. By studying the general three-dimensional case it is easy to see why these are precisely the required forms. To find the strain rate dependent invariants of equation (4), combination invariants of the strain tensor and its time derivative must be considered [28, 29]. The use of these invariants led to the following strain rate dependent invariants:

$$
\begin{aligned}
J_1 &= 2\left(1+2\nu_T\right)\dot{\varepsilon}, & J_6 &= 2\left[\left(2+4\nu_T^2\right)\varepsilon+\left(1-2\nu_T\right)\right]\dot{\varepsilon},\\
J_2 &= 2\left(1+2\nu_T^2\right)\dot{\varepsilon}^2, & J_7 &= 4\left[\left(1+2\varepsilon\right)+2\left(1-2\nu_T\varepsilon\right)\nu_T^2\right]\dot{\varepsilon}^2,\\
J_3 &= 8\nu_T^2\dot{\varepsilon}^3, & J_{10} &= 2\left(1+2\varepsilon\right)\dot{\varepsilon},\\
J_4 &= 2\dot{\varepsilon}, & J_{11} &= 4\left(1+2\varepsilon\right)\dot{\varepsilon}^2,\\
J_5 &= 4\dot{\varepsilon}^2, & J_{12} &= 2\left(1+2\varepsilon\right)^2\dot{\varepsilon}
\end{aligned}
\tag{4}
$$

Being the SEDF expressible in terms of the above invariants: $w(\varepsilon,\dot{\varepsilon}) = \hat{w}(\{I_p, J_q\})$. Then, the equation (2) can be expressed as (5):

$$
\sigma = \sum_{p=1}^{m}\left(\frac{\partial\hat{w}}{\partial I_p}\frac{\partial I_p}{\partial\varepsilon}\right) + \sum_{q=1}^{n}\left(\frac{\partial\hat{w}}{\partial J_q}\frac{\partial J_q}{\partial\varepsilon}\right) \tag{5}
$$

From the preliminary fittings with different polynomial function degrees, it was concluded that the experimental data is more adequately modeled with a polynomial function of fourth degree in ε and degree two in $\dot{\varepsilon}$, these results agree with the results of [10]. Because of this, the specific choice for the SEDF selected for modeling the data is:

$$
\begin{aligned}
w_e(\varepsilon) &= a_1\left(I_1-3\right)^2 + a_2\left(I_5-1\right)^2,\\
w_v(\varepsilon,\dot{\varepsilon}) &= \left(b_1J_1+b_2J_2\right)(I_1-3)^2 + b_3J_5(I_5-1)^2
\end{aligned}
\tag{6}
$$

where the constitutive parameters are a_1, a_2, b_1, b_2 and b_3. Introducing the above SEDF(6) into equation (5), the following explicit equations (7) are obtained:

$$
\begin{aligned}
\sigma_e &= [8(1+2\nu)a_1]\varepsilon + 24[2b_3+4a_2]\varepsilon^2 + [64(a_2+b_3)]\varepsilon^3 = B_1\varepsilon + B_2\varepsilon^2 + B_3\varepsilon^3\\
\sigma_v &= 16\left[b_2(1+2\nu^2)(1+2\nu)^2\dot{\varepsilon}^2 + 2b_1(1+2\nu)^3\dot{\varepsilon}\right]\varepsilon
\end{aligned}
\tag{7}
$$

Therefore, clear viscoelasticity effects would only be found in this model in the linear term, as indeed the data show. In addition, the data manifest that in all cases one has $2b_3 + 4a_2 \approx 0$. With these observations, the above two equations (7) can be put together in a more convenient form simply as the following expression (8):

$$
\sigma = E(\dot{\varepsilon})\varepsilon\left(1-\alpha_1\varepsilon^2\right) \tag{8}
$$

where the effective Young's modulus $E(\dot{\varepsilon})$ and α_1 are given by (9):

$$
\begin{aligned}
E(\dot{\varepsilon}) &= [8(1+2\nu)a_1] + 16[b_2(1+2\nu^2)(1+2\nu)^2\dot{\varepsilon}^2 + 2b_1(1+2\nu)^3\dot{\varepsilon}],\\
\alpha_1 &= 192a_2/E(\dot{\varepsilon})
\end{aligned}
\tag{9}
$$

3 Results

The stress-strain curves obtained from the tensile tests are shown in figure 3. Table 1 contains the anthropometric variables gender, age and body mass index (BMI), as well as the values obtained for the ultimate stress (σ_u), maximum strain ($\varepsilon_{\max}$), the tangent YM and the fitted parameter α_1 (see equation (9)) for all the specimens. Moreover, figure 4 illustrates two typical experimental stress-strain curves resulting from the tensile tests, and the fitted curves obtained with the model proposed in section 2.3. As observed, an excellent good fitting to the model expressed in equation (9) was obtained for all specimens ($r^2 > 0.99$ in all cases, see table 1).

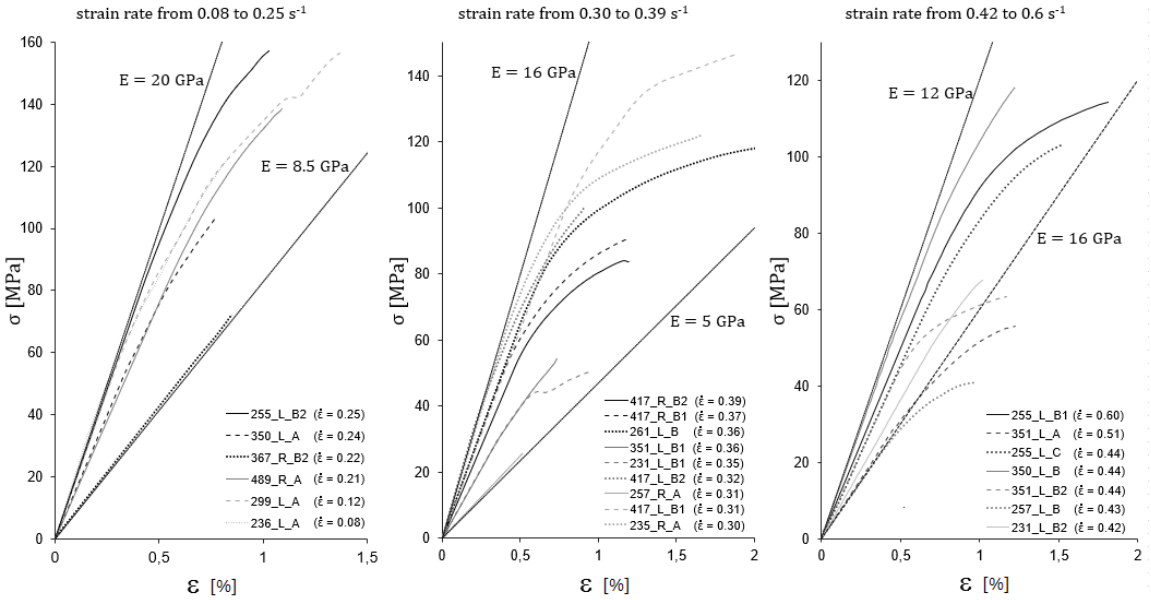

Figure 3: Collection of stress-strain curves for the sample arranged in groups of strain rate.

Figure 5 shows an scatter plot of the YM obtained as a function of the strain rate for each specimen, where a decreasing trend in the values obtained for YM with increasing the strain rate is observed. Statistical analysis of this data set, using the statistical package XLSTAT®, showed that the observed decrease was highly significant ($p-$value < 0.001).

Table 1: Measured values, fitted parameters and anthropometrical variables for all the specimens.

Rib	σ_u	$\varepsilon_{\max}$	$\dot{\varepsilon}$	YM [GPa]	α_1	Gender	Age	BMI	r^2
Rib	[MPa]	[%]	$[s^{-1}]$	[GPa]	[–]		[y.o]	[kg/m^2]	
231-LB1	50.7	0.96	0.35	8.74	0.437	M	85	29.6	0.998
231-LB2	67.7	1.02	0.42	7.48	0.091	M	85	29.6	0.998
235-RA	122	1.65	0.30	14.40	0.553	F	60	32.5	0.997
236-LA	123	0.83	0.08	19.02	0.246	M	79	20.5	0.997
255-LB1	114.2	1.81	0.60	10.35	0.411	M	77	25.0	0.999
255-LB2	157.2	1.03	0.25	20.14	0.235	M	77	25.0	0.999
255-LC	103.4	1.53	0.44	9.46	0.286	M	77	25.0	0.999
257-RA	25.8	0.52	0.31	4.93	0.000	M	71	32.9	0.999
257-LB	40.9	0.98	0.43	6.21	0.331	M	71	32.9	0.999
261-LB	126.6	4.44	0.36	7.69	0.764	M	66	19.8	0.999
299-LA	156.5	1.37	0.12	17.37	0.387	M	56	16.4	0.999
350-LA	103.3	0.77	0.24	16.34	0.183	M	62	29.1	0.999
350-LB	118.4	1.22	0.44	11.91	0.185	M	62	29.1	0.999
351-LA	55.7	1.23	0.51	6.44	0.298	M	89	28.0	0.999
351-LB1	54.6	0.73	0.36	8.50	0.138	M	89	28.0	0.999
351-LB2	63.4	1.17	0.44	9.39	0.456	M	89	28.0	0.999
367-LB	70.0	0.90	0.22	8.52	0.000	M	58	33.4	0.999
417-RB1	91.1	1.20	0.37	12.76	0.448	M	70	21.2	0.998
417-RB2	84.2	1.20	0.39	11.51	0.414	M	70	21.2	0.999
417-LB1	146.8	1.90	0.31	13.22	0.443	M	70	21.2	0.999
417-LB2	100.2	0.91	0.32	15.46	0.307	M	70	21.2	0.999
489-RA	138.9	1.09	0.21	15.93	0.201	M	49	23.3	0.999

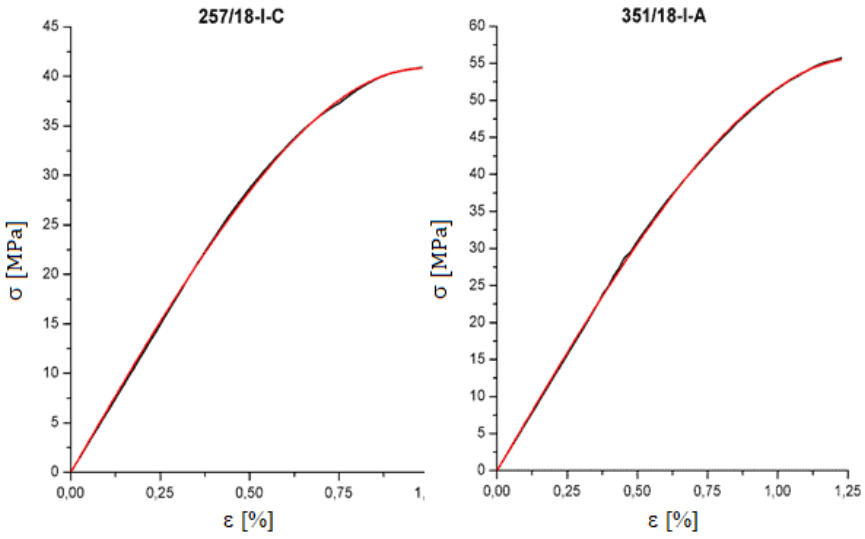

Figure 4: Two examples of fittings of the experimental data to the model. Black lines: measured stress-strain curves, red lines: fitted curves using the proposed model.

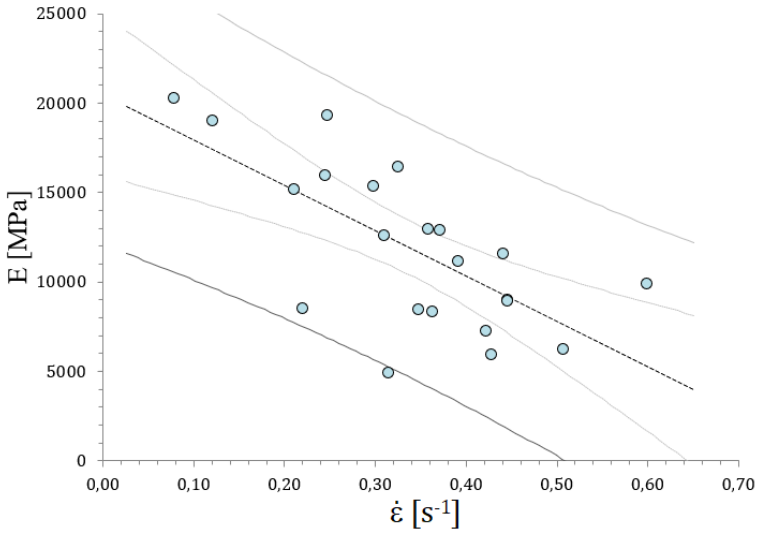

Figure 5: A scatter plot using data of table 1 shows a significant decrease trend with strain rate (p-value < 0.001).

4 Discussion

In this study, the dynamic behavior of human rib cortical bone was investigated, with a focus on analyzing its mechanical properties and proposing a

strain rate dependent model. The most commonly used viscoelastic models were also analyzed. To achieve this, uniaxial tensile tests were conducted on human rib cortical bone specimens at different strain rates. The strain was determined using a Digital Correlation and Tracking (DIC) procedure, which enabled precise strain computation along the entire test without contact with the specimens. Additionally, the real strain rate of each test was determined. From the obtained stress-strain curves, the mechanical properties, including the ultimate stress (σ_u), maximum strain ($\varepsilon_{\max}$) and Young's Modulus (YM), were determined.

The results indicate that YM decreases significantly with increasing strain rate (p-value< 0.001), as observed in some previous studies [5, 8, 19, 20]. However, other studies found no influence of strain rate in YM [14, 15], and moreover older literature indicates that YM increases with strain rate [1, 2].

The occurrence of strain rate dependent phenomena in cortical bone, such as damage or strain rate dependent microcraking, as reported in [22], suggests that purely viscoelastic or viscoplastic models would be insufficient to model the mechanical behavior of cortical bone, and that more complex models that include damage need to be considered, such as the one developed by Schwiedrzik & Zysset [11]. Therefore, under certain conditions, it seems plausible that strain rate dependent factors may exert a greater influence than viscoelastoplastic factors. This possibility could explain the downward trend of YM with strain rate depicted in Figure 5. Zioupos et al. (2008) postulated that the occurrence of microcracks prior to macroscopic failure, which could cause the sample to lose rigidity [22], could be a potential cause of the observed decreasing trend.

Furthermore, as this paper notes, the most frequently used quasi-linear viscoelastic models, such as the standard Maxwell-Wiechert viscoelastic solid model (which is a generalization of the Maxwell model), the Kelvin-Voight model or the Burgers model (which generalizes it) predict that for small strain, the YM should not vary significantly with strain rate as it is shown in Figure 6(b) and appendix 7. Indeed, this seems to be compatible with studies that either do not detect a significant variation [12, 6, 13, 14] or only find very slight variations of YM with the increase of the strain rate [4, 13]. On the other hand, this same figure 6(b) shows that at moderate to large deformations, the slopes of the stress-strain curves do differ more markedly. In fact, since the stress-strain curves for a constant strain rate are concave, the slope of each curve decreases when the strain increases. As observed in

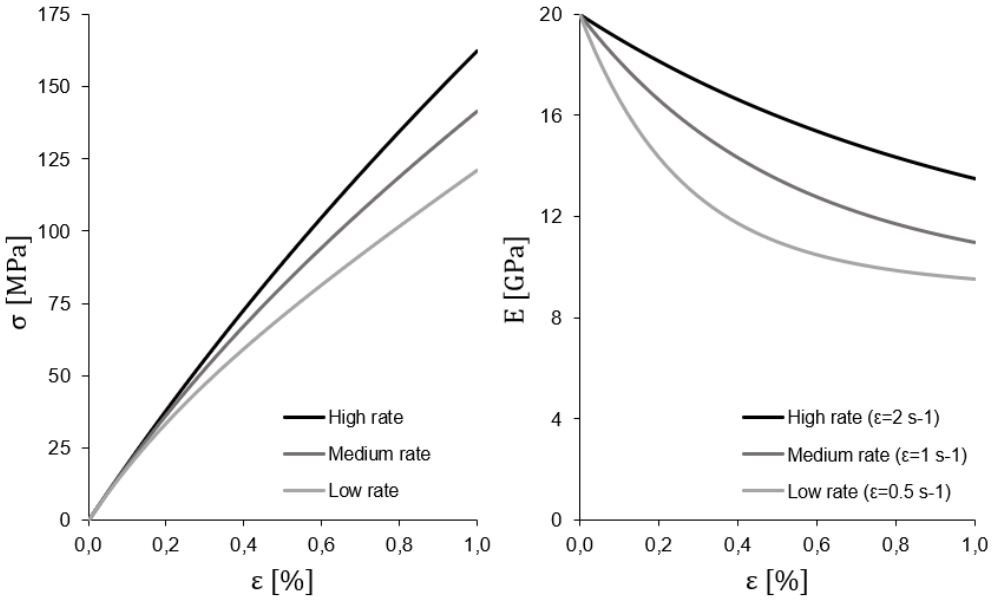

Figure 6: Expected behavior for a generalized Maxwell-Wiechert viscoelastic model: (a) Stress-strain curves at three strain rates ($\dot{\varepsilon} = 0.01,\ 1$ and $10\ s^{-1}$), (b) YM as a function of strain for the same values of strain rate (for $\varepsilon \to 0$ all three YM are the same). All the curves are based on equations (12) and (13) given in the appendix 7, where the values used are $E_0 = 7.6$, $E_1 = 0.4$, $E_2 = 2$, $E_3 = 10$ [GPa], $\tau_1 = 0.5$, $\tau_2 = 0.05$ and $\tau_3 = 0.005$ [s].

the aforementioned figure, this effect is more noticeable for lower than for higher strain rates, so if YM is computed as the average slope over a wide strain range (instead of strictly calculating the tangent YM) it could appear that YM is higher with strain rate, as some articles report [1, 2, 5]. When YM is computed using a wide strain range of the stress-strain curve, it provides a secant YM, not the intrinsic or tangent YM.

It is quite possible, particularly in older studies with analog data acquisition systems, that the YM provided is in fact a secant YM, which could result in an apparent increase in YM with velocity. With more accurate digital acquisition systems and a large number of measurements per second, it is possible to calculate YM with greater precision as a tangent modulus in modern research. This hypothesis would explain why many papers following to the seminal work of McElhaney or Wood did not find such pronounced differences in YM. Previously, other researchers have found inconsistencies or difficulties in McElhaney's work [1]; for instance, in Grames et al. [8] it is

explicitly noted that:
By contrast, the axial constant strain rate results of McElhaney [1] *imply* $\tan\delta \approx 0.15$ *at* 1.6 *Hz, an order of magnitude too high. Such stress-strain curves are graphically appealing; nevertheless, they are inconsistent with the present results as well as with other literature. The discrepancy may result from nonlinear viscoelastic behavior not accounted for in the transformation process, from differences in the bone, or from experimental artifacts.*
Note also that in the review provided by Johnson [9], the two authors who find the most notable and always monotonic YM variations are precisely McElhaney [1] and Wood [2], and it turns out that both use strain gauges mounted directly on the specimens, although this is potentially problematic as other works of the time already indicated [4, 30, 31].

The enormous influence that several of the pioneering papers on strain rate effects in bone [1, 2, 5] had on later literature may explain, in part, why many later researchers who did not find clear or consistent increasing trends in Young's modulus did not explicitly point this out or downplayed those observations. However, there appears to be a wide range of evidence suggesting the existence of flaws, experimental artifacts, or flaws in the way Young's modulus was measured in some of that early work. Thus, when researchers find trends inconsistent with the idea that Young's modulus should increase with strain rate [5, 8, 19, 20], they might have downplayed that finding, so it could be underrepresented in the literature.
Moreover, the prevailing role that the viscoelastic model has had in the study of the mechanical properties of bone should not make us forget that, in fact, there are other strain rate dependent effects that would actually point out that Young's modulus can decrease, although not in certain specific ranges. For example, the strain rate dependent microcracking found by [22] is a phenomenon of this kind which, although it is strain rate dependent, would not fit within the purely viscoelastic or viscoelastoplastic models, see Figure 6). In addition, it is also known that in metallic materials there are phenomena in which the YM can decrease with the strain rate due to alterations in the microstructure, which are favored by the rapid application of loads [34].

Finally, it has to be taken into account, leaving aside the variation of Young's modulus discussed above, that there are other strain rate dependent phenomena which are important for understanding the mechanical properties of bone. For example, another strain rate dependent phenomenon is involved in that the ultimate stress can be affected by the rate of load application.

In fact, the Johnson–Holmquist model represents the mechanical failure of materials that exhibit that characteristic. A case of how these strain rate dependent factors can affect failure is the case of bones subjected to compression, for example in [33], it is analyzed how the fracture of human clavicles subjected to compression present higher failure loads for low load application rates, while in dynamic regime the failure loads tend to be higher in value.

5 Conclusion

Strong experimental evidence has been presented that Young's modulus of cortical bone can decrease with strain rate for some strain rate ranges. This conclusion is supported by those of other authors who found similar results, although due to the lack of an appropriate model and the weight attributed to viscoelastic factors, a systematic explanation has not been attempted. In this paper a phenomenological strain rate dependent model is presented that fits the data, and it has been conjectured that the loss of material stiffness with strain rate within a certain range could be associated to well-characterized phenomena related to the dependence of microcracking on strain rate. The findings of this study may motivate future research to clarify the true mechanisms involved in the decrease of bone Young's modulus with strain rate for small strains, and the development of alternative models that take these mechanisms into account.

The main limitations of this study are given by the limited range of strain rates given by the performance of the testing machine as well as the experimental design, for which a constant maximum strain rate has been ensured throughout the test, and the availability of biological material that meets the established requirements has marked the number of samples as well as their characteristics. As future studies, it would be appropriate to perform the tests with a wider range of strain rates, as well as a larger number of samples with different ages.

6 Acknowledgements

This research was developed within the studies of the research project HERSACA in which both UPM (Madrid) and UPC (Barcelona) participated. The

project was supported with funding from Ministry of Science and Innovation, Spain (No. Grant TRA2016-77979-R).

References

[1] McElhaney, James H. (1996). "Dynamic response of bone and muscle tissue." *J Appl Physiol*, **21**(4), pp. 1231–6.

[2] Wood, J. L. (1971). "Dynamic response of human cranial bone." *Journal of Biomechanics*, **4**(1), pp. 1–12.

[3] Tennyson, R. C., R. Ewert, and V. Niranjan (1972). "Dynamic viscoelastic response of bone." *Experimental Mechanics*, **12**(11), pp. 502–507.

[4] Crowninshield, R. D., & M. H. Pope (1974). "The response of compact bone in tension at various strain rates." *Annals of Biomedical Engineering*, 2(2), pp. 217–225.

[5] Wright, T. M., & Hayes, W. C. (1976). "Tensile testing of bone over a wide range of strain rates: effects of strain rate, microstructure and density." *Medical and biological engineering*, **14**(6), pp. 671–680.

[6] Melnis, A. E., & Knets, I. V. (1982). "Effect of the rate of deformation on the mechanical properties of compact bone tissue." *Mechanics of Composite Materials*, **18**(3), pp. 358–363.

[7] Sasaki, N., & Enyo, A. (1995). "Viscoelastic properties of bone as a function of water content." *Journal of Biomechanics*, **28**(7), pp. 809-815.

[8] Garner, E., Lakes, R., Lee, T., Swan, C., & Brand, R. (2000). "Viscoelastic dissipation in compact bone: implications for stress-induced fluid flow in bone." *J. Biomech. Eng.*, **122**(2), pp. 166–172.

[9] Johnson, T. P. M., Socrate, S.,& Boyce M. C. (2010). "A viscoelastic, viscoplastic model of cortical bone valid at low and high strain rates." *Acta biomaterialia*, **6**(10), pp. 4073–4080.

[10] Pawlikowski, M. (2012). "Cortical bone tissue viscoelastic properties and its constitutive equation-preliminary studies." *Archive of Mechanical Engineering*, **59**(1), pp. 31-52.

[11] Schwiedrzik, J. J., & Zysset, P. K. (2013). "An anisotropic elastic-viscoplastic damage model for bone tissue. Biomechanics and modeling in mechanobiology", **12**(2), pp. 201–213.

[12] Currey, J. D. (1975). "The effects of strain rate, reconstruction and mineral content on some mechanical properties of bovine bone." *Journal of Biomechanics*, **8**(1), pp. 81–86.

[13] Katsamanis, F., Raftopoulos, D.D. (1990). "Determination of mechanical properties of human femoral cortical bone by the Hopkinson bar stress technique." *J Biomech*, **23**(11), pp. 1173–84.

[14] Pithioux, M., Subit, D., & Chabrand, P. (2004). "Comparison of compact bone failure under two different loading rates: experimental and modelling approaches." *Medical engineering & physics*, **26**(8), pp. 647-653.

[15] Katzenberger, M. J., Albert, D. L., Agnew, A. M., & Kemper, A. R. (2020). "Effects of sex, age, and two loading rates on the tensile material properties of human rib cortical bone." *Journal of the mechanical behavior of biomedical materials*, **102**, 103410.

[16] Barrett, J. M., Fewster, K. M., Cudlip, A. C., Dickerson, C. R., & Callaghan, J. P. (2021). "The rate of tendon failure in a collagen fibre recruitment-based model." *Journal of the Mechanical Behavior of Biomedical Materials*, **115**, 104273.

[17] García-Vilana, S., Sánchez-Molina, D., Llumà, J., Galtés, I., Velázquez-Ameijide, J., Rebollo-Soria, M. C., & Arregui-Dalmases, C. (2021). *Viscoelastic characterization of parasagittal bridging veins and implications for traumatic brain injury: a pilot study.* Bioengineering, 8(10), 145.

[18] Hansen, U., Zioupos, P., Simpson, R., Currey, J. D., & Hynd, D. (2008). "The effect of strain rate on the mechanical properties of human cortical bone." *Journal of biomechanical engineering*, **130**(1).

[19] Kirkpatrick, S. J., & Brooks, B. W. (1998). "Micromechanical behavior of cortical bone as inferred from laser speckle data." *Journal of Biomedical Materials Research: An Official Journal of The Society for Biomaterials, The Japanese Society for Biomaterials, and the Australian Society for Biomaterials*, **39**(3), pp. 373–379.

[20] Adharapurapu, R. R., Jiang, F.,& Vecchio, K. S. (2006). "Dynamic fracture of bovine bone." *Materials Science and Engineering: C*, **26**(8), pp. 1325–1332.

[21] Wayne Chen, W., Jane Wang, Q., Huan, Z., & Luo, X. (2011). "Semi-analytical viscoelastic contact modeling of polymer-based materials." *Journal of Tribology*, **133**(4).

[22] Zioupos, P., Hansen, U., & Currey, J. D. (2008). "Microcracking damage and the fracture process in relation to strain rate in human cortical bone tensile failure. Journal of Biomechanics, **41**(14), pp. 2932–39.

[23] Sanchez-Molina, D., Velazquez-Ameijide, J., Quintana, V., Arregui-Dalmases, C., Crandall, J. R., Subit, D., & Kerrigan, J. R.: "Fractal dimension and mechanical properties of human cortical bone". *Medical engineering & physics*, **35** (5), pp. 576–582, 2013.

[24] Velázquez-Ameijide, J., García-Vilana, S., Sánchez-Molina D, Llumà-Fuentes, J., Martínez-González, E., Rebollo-Soria, M.C., & Arregui-Dalmases, C. (2020): "Prediction of mechanical properties of human rib cortical bone using fractal dimension". *Computer Methods in Biomechanics and Biomedical Engineering*, 1–11.

[25] Velázquez-Ameijide, J., García-Vilana, S., Sánchez-Molina D, Martínez-González, E., Llumà-Fuentes, J., Rebollo-Soria, M.C., & Arregui-Dalmases, C. (2021): "Influence of anthopometric variables on the mechanical properties of human rib cortical bone." *Biomedical Physics & Engineering Express*, **7**(3), 035013.

[26] Coleman, B. D., & Gurtin, M. E. (1967). "Thermodynamics with internal state variables." *The journal of chemical physics*, **47**(2), pp. 597–613.

[27] Holzapfel, A. G. (2000). *Nonlinear Solid Mechanics: A Continuum Approach for Engineering Science*, John Wiley & Sons, Chichester2000. ISBN: 0-471-82319-8

[28] Zheng, Q. S., & Boehler, J. P. (1994). "The description, classification, and reality of material and physical symmetries." *Acta Mechanica*, **102**(1), pp. 73–89.

[29] Limbert, G., & Middleton, J. (2004). "A transversely isotropic viscohyperelastic material: Application to the modeling of biological soft connective tissues." *International Journal of Solids and Structures*, **41**(15), pp. 4237–4260.

[30] Burstein, A. H., & Frankel, V. H. (1968). The viscoelastic properties of some biological materials. Annals of the New York Academy of Sciences, 146(1), 158-165.

[31] Sammarco, G. J., Burstein, A. H., Davis, W. L., & Frankel, V. H. (1971). "The biomechanics of torsional fractures: the effect of loading on ultimate properties." *Journal of biomechanics*, **4**(2), pp. 113–117.

[32] Johnson, G.R., Holmquist, T. J. (1994). "An improved computational constitutivemodel for brittle materials." *AIP Conference Proceeding*, pp. 309–981.

[33] Sánchez-Molina, D., García-Vilana, S., Velázquez-Ameijide, J. & Arregui-Dalmases, C. (2020) "Probabilistic assessment for clavicle fracture under compression loading: rate-dependent behavior." *Biomedical Engineering: Applications, Basis and Communications* **32**(5), 2050040.

[34] Kommel, L. (2019). "Microstructure and properties that change during hard cyclic visco-plastic deformation of bulk high purity niobium." em International Journal of Refractory Metals and Hard Materials, **79**, pp. 10-17.

[35] Morro, A. (2017). "Modelling of viscoelastic materials and creep behaviour." *Meccanica*, **52**(13), pp. 3015–3021.

7 Appendix: Viscoelastic computations

A general justification of the insensibility of tangent Young's modulus is presented in this section. For this purpose a generalized Wiechert-Maxwell viscoelastic model is considered (this model is commonly used in modeling of biological tissues). It will be shown that for small strains, it would not be possible to find appreciable differences in Young's modulus, just as many authors find [6, 12, 13, 14, 15]. This conclusion is also valid for other types of viscoelastic models, including non-QLVE models, although this justification

is more complex and will not be dealt with in this appendix.
The Wiechert-Maxwell model appears as a combination of rate-dependent mechanisms which can be represented symbolically schematically as in figure 7. This model is a QLVE model given by a differential equation (10) of order n in $\sigma(t)$ and $\varepsilon(t)$, as deduced from [35]:

$$\sigma + \alpha_1 \frac{\partial \sigma}{\partial t} + \cdots + \alpha_n \frac{\partial^n \sigma}{\partial t^n} = E_0 \varepsilon + \beta_1 \frac{\partial \varepsilon}{\partial t^n} + \cdots + \beta_n \frac{\partial^n \varepsilon}{\partial t^n} \tag{10}$$

where the constants $\alpha_i = \alpha_i(\{E_k/E_k\})$ and $\beta_i = \beta_i(E_0, \{E_k, \eta_k\})$ are always expressible in terms of the viscosities $\eta_k \geq 0$ and the stiffnesses $E_k > 0$. For a

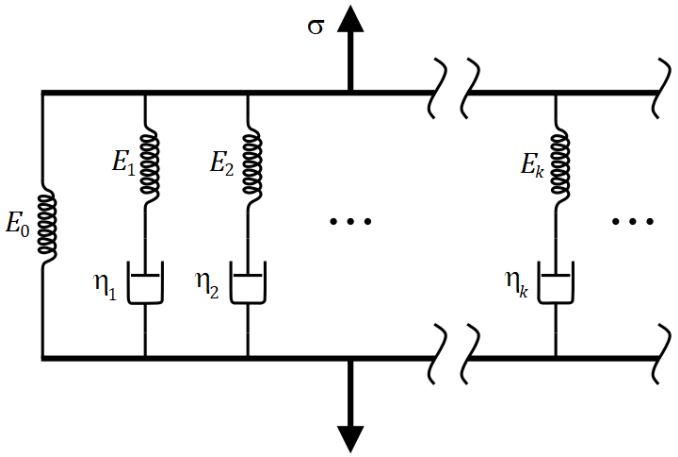

Figure 7: Equivalent diagram in terms of springs and dampers for Wiechert-Maxell model. The parameters E_i and η_j are intrinsic parameters of the model, from they the characteristic time scales are derived $\tau_k = \eta_k/E_k$ for $1 \leq k \leq n$.

deformation process where $\sigma(0) = 0$ when $\varepsilon(0) = 0$, the integration by Laplace transformatin method leads to the following form (11):

$$\sigma(t) = E_0 \varepsilon(t) + \sum_{k=1}^{n} E_k \int_0^t e^{-\frac{t-\xi}{\tau_k}} \frac{\mathrm{d}\varepsilon(\xi)}{\mathrm{d}\xi} \, \mathrm{d}\xi \tag{11}$$

where $\tau_k = \eta_k/E_k$. This expression is equivalent to equation (3) used in [21]. For a loading process with constant strain rate $t = \varepsilon/\dot{\varepsilon}$ the last expression becomes as the following equation (12):

$$\sigma = E_0 \varepsilon + \dot{\varepsilon} \sum_{k=1}^{n} E_k \tau_k \left[1 - e^{-\varepsilon/(\dot{\varepsilon}\tau_k)}\right] \tag{12}$$

Given a certain level of strain ε, the stress grows with strain rate, since $\partial\sigma/\partial\dot{\varepsilon} > 0$ (Figure 6(a)). In addition, the slope of the stress-strain curve is given by (13):

$$E_\varepsilon = \frac{\partial\sigma}{\partial\varepsilon} = E_0 + \sum_{k=1}^{n} E_k \left[1 - e^{-\varepsilon/(\dot{\varepsilon}\tau_k)}\right] \tag{13}$$

Therefore, the Young's modulus tangent E_{tan} is precisely:

$$E_{tan} = \lim_{\varepsilon\to 0} E_\varepsilon = E_0 + E_1 + \cdots + E_n \tag{14}$$

and, as it can be seen in (14), is independent of the strain rate.
Figure 6 shows an example of mechanical properties of the Wiechert-Maxwell model ($n = 3$) with $E_0 = 7.6$, $E_1 = 0.4$, $E_2 = 2$, $E_3 = 10$ [GPa], $\tau_1 = 0.5$, $\tau_2 = 0.05$ and $\tau_3 = 0.005$ [s], and the selected strain rates are $\dot{\varepsilon_0}$ are 2, 1 and 0.5 [s^{-1}]. In particular, the 6(b) shows that the Young's modulus for very small strains tends to the same value irrespective of the velocity, i.e., the tangent Young's modulus does not depend on the strain rate.

8 Appendix: 3D-generalisation of the model

For the 3D generalization of the uniaxial model of section 2.3, we will use the same procedure of Coleman and Noll [26, 27], but we will use full tensorial forms. Instead of using ε as the strain measure, the right Cauchy–Green deformation tensor $\mathbf{C}$ is used intead. As in the 1D case, a descomposition of the SEDF in purely elastic and strain rate dependent parts is assumed $W(\mathbf{C}, \dot{\mathbf{C}}) = W_e(\mathbf{C}) + W_v(\mathbf{C}, \dot{\mathbf{C}})$. In this case we will use the Second Piola–Kirchhoff stress tensor $\mathbf{S} = (S_{ij})$ as a mesure of the stress, in equation (15). The relation is similar to that found in equation (2):

$$S_{ij} = 2\frac{\partial W}{\partial C_{ij}} \tag{15}$$

Now, again, it is a matter of choosing the appropriate invariants, according to the *objectivity principle*. In this case, algebraic invariants formed with the tensors $\mathbf{C}$ and $\dot{\mathbf{C}}$. The purely elastic invariants are (16):

$$\begin{aligned} I_1 &= \text{tr } \mathbf{C}, & I_4 &= \mathbf{N}_0 : \mathbf{C} \\ I_2 &= \tfrac{1}{2}(\text{tr}^2\ \mathbf{C} - \text{tr } \mathbf{C}^2), & I_5 &= \mathbf{N}_0 : \mathbf{C}^2 \\ I_3 &= \det(\mathbf{C}) - 1 \end{aligned} \tag{16}$$

where $\mathbf{N}_0 := \boldsymbol{n}_0 \otimes \boldsymbol{n}_0$ being $\boldsymbol{n}_0$ the vector direction of the preferred (longitudinal) direction at each point of the transversely isotropic material. In addition to the above invariants (16), we have the mixed strain rate dependent invariants (17) [10, 29]:

$$\begin{array}{lll} J_1 = \mathrm{tr}\ \dot{\mathbf{C}}, & J_5 = \mathbf{N}_0 : \dot{\mathbf{C}}^2, & J_9 = \mathrm{tr}(\mathbf{C}^2 \cdot \dot{\mathbf{C}}^2), \\ J_2 = \mathrm{tr}\ \dot{\mathbf{C}}^2/2, & J_6 = \mathrm{tr}(\mathbf{C} \cdot \dot{\mathbf{C}}), & J_{10} = \mathrm{tr}(\mathbf{N}_0 \cdot \mathbf{C} \cdot \dot{\mathbf{C}}), \\ J_3 = \det\ \dot{\mathbf{C}}, & J_7 = \mathrm{tr}(\mathbf{C} \cdot \dot{\mathbf{C}}^2), & J_{11} = \mathrm{tr}(\mathbf{N}_0 \cdot \mathbf{C} \cdot \dot{\mathbf{C}}^2), \\ J_4 = \mathbf{N}_0 : \dot{\mathbf{C}}, & J_8 = \mathrm{tr}(\mathbf{C}^2 \cdot \dot{\mathbf{C}}), & J_{12} = \mathrm{tr}(\mathbf{N}_0 \cdot \mathbf{C}^2 \cdot \dot{\mathbf{C}}) \end{array} \tag{17}$$

The same argumentation that preceded the equation (6) leads now to choose the functions $W_e(\mathbf{C})$ and $W_v(\mathbf{C}, \dot{\mathbf{C}})$ as (18):

$$\begin{array}{ll} W_e(\mathbf{C}) & = a_1 \left(I_1 - 3\right)^2 + a_2 \left(I_5 - 1\right)^2 \\ W_v(\mathbf{C}, \dot{\mathbf{C}}) & = \left(b_1 J_1 + b_2 J_2\right) \left(I_1 - 3\right)^2 + b_3 J_5 \left(I_5 - 1\right)^2 \end{array} \tag{18}$$